

# The Mobility of a Conserved Tyrosine Residue Controls Isoform-Dependent Enzyme–Inhibitor Interactions in Nitric Oxide Synthases

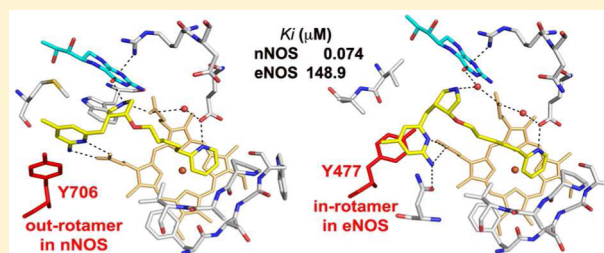
Huiying Li,<sup>†</sup> Joumana Jamal,<sup>†</sup> Silvia Delker,<sup>†,§</sup> Carla Plaza,<sup>†</sup> Haitao Ji,<sup>‡,||</sup> Qing Jing,<sup>‡</sup> He Huang,<sup>‡</sup> Soosung Kang,<sup>‡</sup> Richard B. Silverman,<sup>\*,‡</sup> and Thomas L. Poulos<sup>\*,†</sup>

<sup>†</sup>Departments of Molecular Biology and Biochemistry, Pharmaceutical Sciences, and Chemistry, University of California, Irvine, California 92697-3900, United States

<sup>‡</sup>Department of Chemistry, Department of Molecular Biosciences, Chemistry of Life Processes Institute, and Center for Molecular Innovation and Drug Discovery, Northwestern University, 2145 Sheridan Road, Evanston, Illinois 60208-3113, United States

## Supporting Information

**ABSTRACT:** Many pyrrolidine-based inhibitors highly selective for neuronal nitric oxide synthase (nNOS) over endothelial NOS (eNOS) exhibit dramatically different binding modes. In some cases, the inhibitor binds in a 180° flipped orientation in nNOS relative to eNOS. From the several crystal structures we have determined, we know that isoform selectivity correlates with the rotamer position of a conserved tyrosine residue that H-bonds with a heme propionate. In nNOS, this Tyr more readily adopts the out-rotamer conformation, while in eNOS, the Tyr tends to remain fixed in the original in-rotamer conformation. In the out-rotamer conformation, inhibitors are able to form better H-bonds with the protein and heme, thus increasing inhibitor potency. A segment of polypeptide that runs along the surface near the conserved Tyr has long been thought to be the reason for the difference in Tyr mobility. Although this segment is usually disordered in both eNOS and nNOS, sequence comparisons and modeling from a few structures show that this segment is structured quite differently in eNOS and nNOS. In this study, we have probed the importance of this surface segment near the Tyr by making a few mutants in the region followed by crystal structure determinations. In addition, because the segment near the conserved Tyr is highly ordered in iNOS, we also determined the structure of an iNOS–inhibitor complex. This new structure provides further insight into the critical role that mobility plays in isoform selectivity.



In an  $\text{O}_2^-$ - and nicotinamide adenine dinucleotide phosphate-dependent reaction, nitric oxide synthase oxidizes L-arginine to L-citrulline and the important signaling molecule nitric oxide (NO).<sup>1</sup> Mammals produce three NOS isoforms: neuronal NOS (nNOS), inducible NOS (iNOS), and endothelial NOS (eNOS). Each isoform participates in fundamental physiological functions in the nervous, immune, and cardiovascular systems.<sup>2</sup> The over- and underproduction of NO is associated with various disease states; consequently, the development of NOS inhibitors is an important therapeutic goal.<sup>3</sup> The focus of our research efforts<sup>4,5</sup> has been the development of nNOS selective inhibitors that can be used in treating neurodegenerative diseases, such as Alzheimer's, Parkinson's, and Huntington's diseases.<sup>6</sup> Isoform selectivity, however, is critical because blocking eNOS would interfere with the role NO plays in maintaining vascular tone and blood pressure.<sup>7</sup>

Achieving high isoform selectivity has been a challenge because the active sites of all three NOS isoforms are very similar.<sup>8–11</sup> Our previous work<sup>12</sup> showed that a single amino acid difference, Asp597 in nNOS versus Asn368 in eNOS, is responsible for the ability of nNOS to bind a series of dipeptide inhibitors much more tightly than does eNOS.<sup>13,14</sup> Accumulated structural information formed the basis for a fragment-based

inhibitor design approach resulting in pyrrolidine-containing inhibitors, which showed excellent potency and selectivity for nNOS over eNOS.<sup>15</sup>

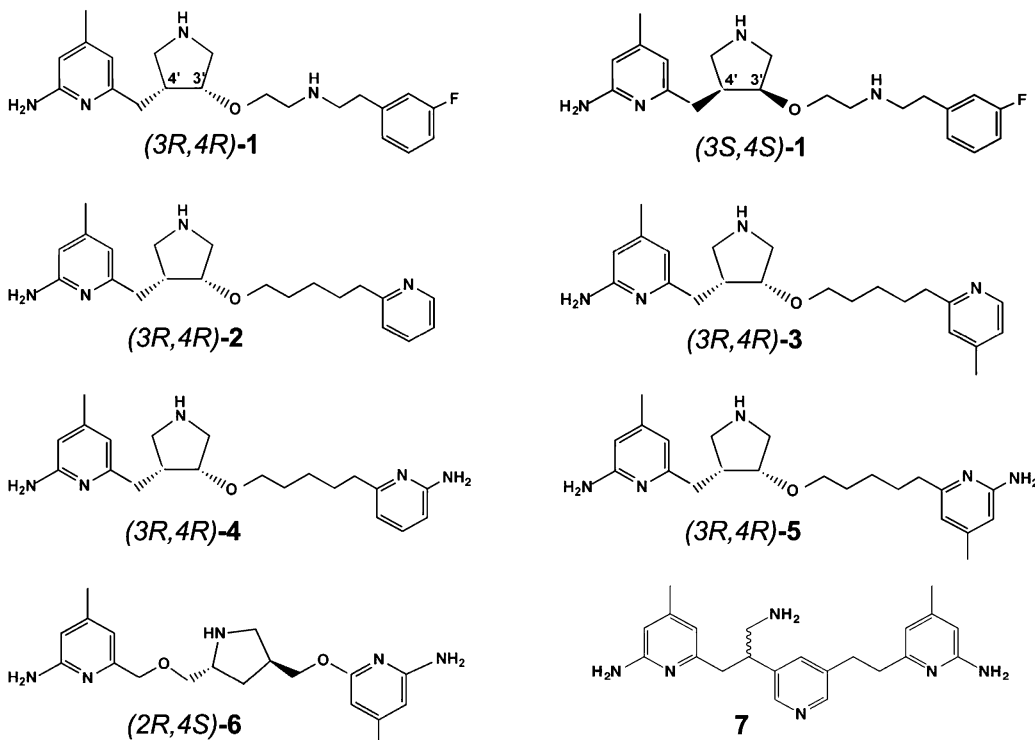
Chirality at the 3' and 4' positions of compounds such as **1** (Table 1) proved to be critically important for both potency and selectivity. (3S,4S)-**1** has the aminopyridine positioned in the active site where it interacts with Glu592 of nNOS, while Tyr706 is in its in-rotamer position. However, the more potent and selective (3R,4R)-**1** binds in a 180° flipped mode with the aminopyridine moiety H-bonding to heme propionate D and Tyr706 adopting an out-rotamer conformation to make this binding mode feasible (Figure 1).<sup>16,17</sup> These two binding possibilities have been achieved with a single compound that bears double-headed aminopyridine groups.<sup>18,19</sup> We have recently developed more pyrrolidine-based nNOS inhibitors, such as compounds (3R,4R)-**2** and (3R,4R)-**3** in Table 1, that target heme propionate D and exhibit 2000- and 1400-fold selection for nNOS versus eNOS, respectively.<sup>20</sup> The crystal structures revealed that these inhibitors interact with heme

Received: May 10, 2014

Revised: July 25, 2014

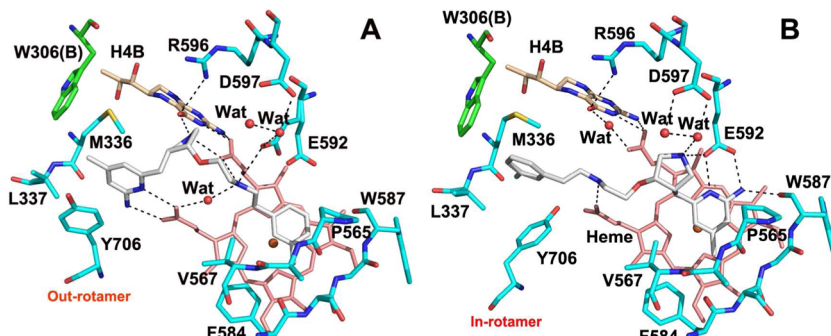
Published: August 4, 2014

Table 1. Potencies and Selectivities of the NOS Inhibitors Discussed in This Study



compound	$K_i$ ( $\mu\text{M}$ ) <sup>a</sup>			selectivity <sup>b</sup>		refs
	nNOS	eNOS	iNOS	n/e	n/i	
(3R,4R)-1	0.0072	19.2	5.8	2667	806	17
(3S,4S)-1	0.116	26.2	7.5	226	65	17
(3R,4R)-2	0.074	148.9	9.8	2012	132	20
(3R,4R)-3	0.031	45.2	17.3	1459	558	20
(3R,4R)-4	0.030	33.5	18.6	1117	619	20
(3R,4R)-5	0.038	26.1	6.5	687	172	20
(2R,4S)-6	0.0097	6.7	2.9	693	295	32
racemic 7	0.030	16.0	2.8	544	95	33, 34

<sup>a</sup>The apparent  $K_i$  values are represented as the means of two or more independent experiments in 100 mM HEPES buffer (pH 7.5) performed in duplicate with five or six data points each.<sup>20</sup> <sup>b</sup>n/e and n/i are the selectivity ratios of  $K_i$  (eNOS or iNOS) to  $K_i$  (nNOS).



**Figure 1.** Two different modes of binding of 1 to nNOS depending on the chirality at positions 3' and 4' of the pyrrolidine. (A) (3R,4R)-1 (PDB entry 3NLM<sup>17</sup>) with its aminopyridine H-bonded with heme propionate D while Tyr706 is in an out-rotamer position. (B) (3S,4S)-1 (PDB entry 3NLK<sup>17</sup>) with its aminopyridine H-bonded with Glu592 while Tyr706 is in an in-rotamer position. All figures were prepared with PyMol (<http://www.pymol.org>).

propionate D in nNOS with a conformation different from that in eNOS, mainly because a conserved Tyr residue, Tyr477 in nNOS versus Tyr477 in eNOS, is able to adopt an out-rotamer conformation more easily in nNOS than in eNOS. This movement of the conserved Tyr is necessary to allow the

inhibitor aminopyridine group to form tight bifurcated H-bonds with heme propionate D. The aim of this study is to determine whether the Tyr rotamer position is the sole determinant of isoform selectivity and identify the structural basis underlying the Tyr rotamer preference in nNOS versus eNOS.

**Table 2.** Spectral Binding Constants ( $K_s$ , in micromolar) Determined with the NOS Heme Domain Proteins at 25 °C<sup>a</sup>

inhibitor	(3R,4R)-2	(3R,4R)-3	(2R,4S)-6	7
wild type nNOS	0.212 ± 0.045	0.198 ± 0.018	0.050 ± 0.006	0.030 ± 0.004
nNOS M336V/D597N	1.93 ± 0.12	0.393 ± 0.024	0.153 ± 0.023	0.265 ± 0.029
nNOS H341L	N/D <sup>b</sup>	N/D <sup>b</sup>	0.352 ± 0.018	0.632 ± 0.198
wild type eNOS	41.3 ± 3.5	55.8 ± 6.4	1.60 ± 0.17	10.6 ± 1.9
eNOS Y477A	N/D <sup>b</sup>	N/D <sup>b</sup>	3.49 ± 0.24	15.4 ± 1.2
eNOS L111A	N/D <sup>b</sup>	7.27 ± 0.32	1.18 ± 0.29	N/D <sup>b</sup>
human iNOS	N/D <sup>b</sup>	N/D <sup>b</sup>	N/D <sup>b</sup>	1.19 ± 0.29

<sup>a</sup>Details of the titration conditions are described in Experimental Procedures. Titration of the rat nNOS (or bovine eNOS) heme domain with each inhibitor was conducted in duplicate so that the mean  $K_s$  and the standard deviation could be reported in this table. <sup>b</sup>Not determined.

## ■ EXPERIMENTAL PROCEDURES

**Preparation of Bovine eNOS L111A and Y477A and Rat nNOS H341L and M336V/D597N Mutants.** Three different point mutations, eNOS L111A, eNOS Y477A, and nNOS H341L, were prepared by the QuikChange protocol (Stratagene) via polymerase chain reaction using the pCWori vector as the template, which contains the gene of the corresponding full length wild type eNOS or nNOS. The resulting plasmids with the mutation were confirmed by sequencing of the entire coding region. The preparation of the rat nNOS double mutant, M336V/D597N, was as reported previously.<sup>12</sup> Protein expression and purification of these full length eNOS or nNOS mutants were conducted using the established procedure reported previously.<sup>9,11</sup> The heme domain samples used for structural studies were generated by limited trypsinolysis of full length eNOS or nNOS, and the resulting fragments of the heme domain and FAD-containing domain were further separated by a Superdex 200 gel filtration column, as described previously.<sup>9,11</sup>

**Inhibitor Complex Crystal Preparation.** The rat nNOS heme domain (9 mg/mL, containing 20 mM histidine) or the bovine eNOS heme domain (12 mg/mL, containing 2 mM imidazole) was used for sitting drop vapor diffusion crystallization. Diffraction quality crystals were obtained after incubation for 2 days at 4 °C over the following reservoir solutions: for nNOS, 20–24% PEG3350, 100 mM MES (pH 5.8), 140–200 mM ammonium acetate, 10% ethylene glycol, 5 mM GSH, and 35 μM SDS; for eNOS, 18–22% PEG3350, 100 mM cacodylate (pH 6.0), 150–200 mM magnesium acetate, and 5 mM TCEP. Fresh crystals were first passed stepwise through cryoprotectant solutions as described previously<sup>9,11</sup> and then soaked with 10 mM inhibitor for 4–6 h at 4 °C before being flash-cooled with liquid nitrogen.

**Spectral Binding Constants.** In addition to the known inhibitory constants ( $K_i$  in Table 1) obtained with the wild type rat nNOS or bovine eNOS full length enzymes, we also determined the spectral binding constants of inhibitors bound to the heme domain, wild type or mutants, which are the same samples used to obtain crystal structures. All of the inhibitors in this study are high-spin, type I inhibitors. The buffer consisted of 50 mM HEMES (pH 7.5), 10% glycerol, and 100 mM NaCl, containing 1 mM imidazole (a low-spin, type II ligand). Inhibitor binding displaces the imidazole, resulting in a well-defined shift in the spectrum from low- to high-spin. The spectral shift was monitored for a few minutes at room temperature after each addition of increasing amounts of inhibitor to 5–6 μM protein. The differences in absorbance between the peak (390 nm) and trough (430 nm) were plotted against the inhibitor concentration. The data showing weaker binding to eNOS were usually fit well using SigmaPlot (Systat Software Inc.) with a hyperbolic one-site ligand binding equation. However, for inhibitors that

bound more tightly to nNOS, a quadratic equation was needed for better fitting (Figure S1 of the Supporting Information).<sup>21</sup> The apparent  $K_s$  constants [ $K_s(\text{app})$ ] were further converted to  $K_s$  via the equation  $K_s(\text{app}) = K_s(1 + [\text{imidazole}]/K_{d,\text{imidazole}})$  and are listed in Table 2. The  $K_d$  values of imidazole for nNOS, eNOS, and iNOS are 160 μM,<sup>22</sup> 150 μM,<sup>23</sup> and 42 μM,<sup>24</sup> respectively.

**X-ray Diffraction Data Collection, Data Processing, and Structural Refinement.** The cryogenic (100 K) X-ray diffraction data were collected remotely at the Stanford Synchrotron Radiation Lightsource (SSRL) or Advanced Light Source (ALS) through the data collection control software Blu-Ice<sup>25</sup> and a crystal mounting robot. Raw CCD data frames were indexed, integrated, and scaled using HKL2000.<sup>26</sup> The human iNOS diffraction data were collected at BL11-1 of SSRL using a Pilatus pixel array detector. The finely sliced (0.2° per frame) and highly redundant (160° in scanning angle) data were processed with XDS<sup>27</sup> and scaled with Scala.<sup>28</sup> Binding of inhibitors was detected by the initial difference Fourier maps calculated with REFMAC.<sup>29</sup> The inhibitor molecules were then modeled in COOT<sup>30</sup> and refined using REFMAC. Disorder in portions of inhibitors bound in the NOS active sites was often observed, sometimes resulting in poor density quality. However, partial structural features usually could still be visible if the contour level of the sigmaA-weighted  $2m|F_o| - |F_c|$  map dropped to 0.5σ, which afforded the building of reasonable models into the disordered regions. Water molecules were added in REFMAC and checked by COOT. The TLS<sup>31</sup> protocol was implemented in the final stage of refinements with each subunit as one TLS group. The omit  $F_o - F_c$  density maps were calculated by repeating the last round of TLS refinement with the inhibitor coordinate removed from the input PDB file to generate the map coefficients DELFWT and PHDELWT. The refined structures were validated in COOT before deposition in the PDB. The crystallographic data collection and structure refinement statistics are summarized in Table S1 of the Supporting Information, with the PDB codes included.

## ■ RESULTS AND DISCUSSION

**Binding of (3R,4R)-Pyrrolidine Inhibitors to nNOS.** Chemical structures of the compounds discussed in this study as well as their inhibitory potencies and selectivities are listed in Table 1. To directly correlate the ligand binding affinity and the binding mode found in structures, the spectral binding constants of four compounds with various heme domain proteins are listed in Table 2. Compared to the parental inhibitor (3R,4R)-1, both (3R,4R)-2 and (3R,4R)-3 have the tail end hydrophobic phenyl ring replaced with a pyridine ring to introduce hydrogen bonds between the inhibitor and protein. These two inhibitors show good potency and high selectivity for nNOS over eNOS (Table

1). As we have reported,<sup>20</sup> the two (3*R*,4*R*)-inhibitors, 2 and 3, bind to nNOS (Figure 2) with the aminopyridine ring hydrogen

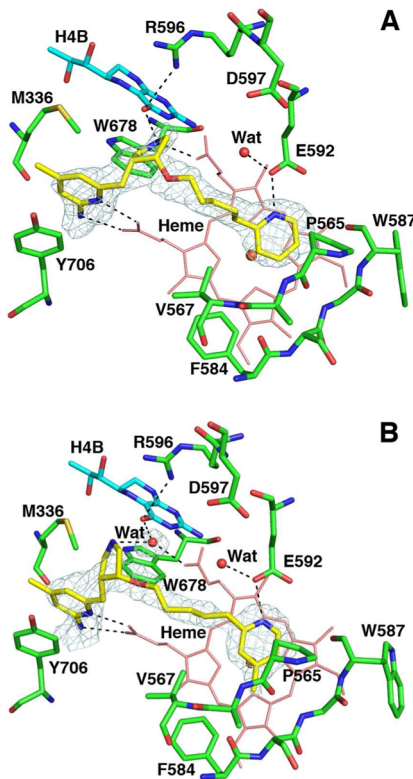


**Figure 2.** NNOS active site bound with (A) (3*R*,4*R*)-2 (PDB entry 3UFU<sup>20</sup>) and (B) (3*R*,4*R*)-3 (PDB entry 3UFV<sup>20</sup>). The omit  $F_o - F_c$  density map for each inhibitor is shown at the  $3.0\sigma$  contour level. Major hydrogen bonds are depicted as dashed lines.

bonded to heme propionate D and stacked with the Tyr706 side chain in its out-rotamer position. The pyridine ring at the other end of the inhibitor hydrogen bonds with Glu592. There are some variations with respect to how the pyrrolidine ring interacts with the protein. For (3*R*,4*R*)-2 (Figure 2A), the pyrrolidine ring bends down between heme propionate A and H<sub>4</sub>B, thereby hydrogen bonding to both through its ring nitrogen atom. This pyrrolidine binding position is identical to what has been observed for parental inhibitor (3*R*,4*R*)-1.<sup>16</sup> The pyrrolidine nitrogen atom occupies the position of a water molecule present in the substrate complex structures for both nNOS and eNOS (PDB entries 1OM4 and 2NSE). In the nNOS-3 structure (Figure 2B), however, this water molecule is still present, while the pyrrolidine of (3*R*,4*R*)-3 bends up but contacts the water molecule. Overall, (3*R*,4*R*)-3 adopts a more extended conformation in the linker between the tail pyridine and the pyrrolidine rings, so that the position of the aminopyridine is at least 0.5 Å farther from the nNOS active site than that observed in the nNOS-1 structure. Another difference between (3*R*,4*R*)-2 and (3*R*,4*R*)-3 is the orientation of the tail pyridine ring. In the nNOS-2 structure, the ring is approximately parallel to heme pyrrole A, while the ring in the nNOS-3 structure makes an ~30° tilt from the heme plane. This is most likely because the extra methyl group on the pyridine in (3*R*,4*R*)-3 imposes additional restraints on the ring orientation via its van der Waals contact with the Phe584 side chain. This additional contact may have created a binding affinity of (3*R*,4*R*)-3 slightly tighter than that of (3*R*,4*R*)-2.

**Binding of (3*R*,4*R*)-Inhibitors to eNOS.** Although (3*R*,4*R*)-2 and (3*R*,4*R*)-3 also bind to eNOS (Figure 3) with

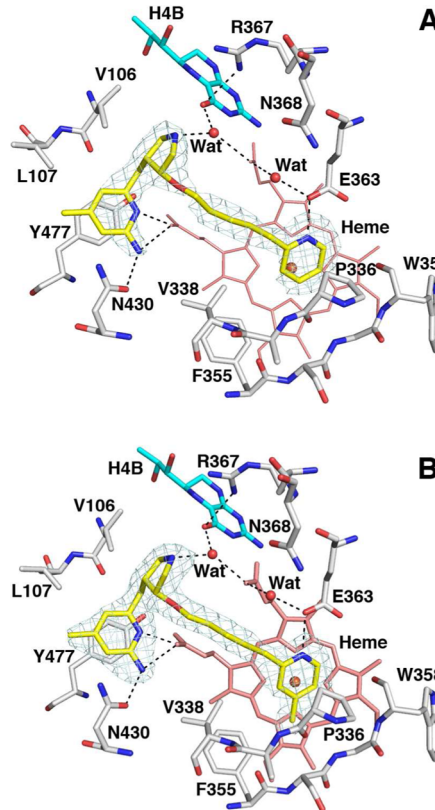


**Figure 3.** ENOS active site bound with (A) (3*R*,4*R*)-2 and (B) (3*R*,4*R*)-3. The omit  $F_o - F_c$  density map for each inhibitor is shown at the  $3.0\sigma$  contour level. Major hydrogen bonds are depicted as dashed lines.

the aminopyridine ring next to heme propionate D, Tyr477 remains in place and does not adopt the out-rotamer position as it does in nNOS. Therefore, the aminopyridine is able to form hydrogen bonds with only one oxygen atom of heme propionate D, whereas the 2-amino group forms an H-bond with Asn340. The pyridine in the tail of either inhibitor makes a hydrogen bond with Glu363 similar to that seen in nNOS. The inability to form direct bifurcated H-bonds with the heme propionate D in eNOS is likely the main reason why (3*R*,4*R*)-2 and (3*R*,4*R*)-3 bind to eNOS more poorly than to nNOS (Tables 1 and 2). Both exhibit the weakest binding to eNOS among the compounds in this study, judging by both  $K_i$  and  $K_s$  (Tables 1 and 2), while (3*R*,4*R*)-2 gives the highest isoform selectivity. A concern was raised during the review about whether it is valid to correlate the inhibitory data ( $K_i$ ), which were determined at pH 7.5 and room temperature, using full length enzymes, directly with the heme domain crystal structures obtained at lower pH values (pH 5.8 for nNOS and pH 6.0 for eNOS) and liquid nitrogen temperature (100 K). The spectral binding constants ( $K_s$ ) determined with the heme domain protein at pH 7.5 and room temperature show a consistent trend with inhibitory  $K_i$  values, which indicates that the enzyme-inhibitor interaction and the accessibility of the inhibitor to the NOS active site are very similar, whether it is in the full length enzyme or the heme domain alone. The NOS heme active site has a wide open channel, which allows the soaking of small molecules into NOS crystals without crystal damage. The temperature issue is hard to

address because the NOS crystal structures at room temperature are not available. The pH effects may not be a concern because the comparison of binding of the ligand to nNOS and eNOS is made in the same pH range (~6.0).

#### More Examples of Isoform-Dependent Binding Modes.

Similar isoform-dependent inhibitor binding modes have been observed with other inhibitors. We have reported<sup>20</sup> that (3*R*,4*R*)-4 and (3*R*,4*R*)-5 bind to nNOS (Figure S2 of the Supporting Information) in a double-headed mode with each of the heads hydrogen bonded with either the Glu592 side chain or heme propionate D. With eNOS, however, the two inhibitors do not form bifurcated hydrogen bonds to heme propionate D with the aminopyridine; instead, the aminopyridine stacks with the Tyr477 side chain that itself remains in the in-rotamer position to hydrogen bond with heme propionate D (Figure S3 of the Supporting Information), which is similar to how (3*R*,4*R*)-2 and (3*R*,4*R*)-3 bind to eNOS (Figure 3). We recently also reported pyrrolidine-based inhibitor (2*R*,4*S*)-6, which provides another example.<sup>32</sup> In nNOS, (2*R*,4*S*)-6 makes hydrogen bonds with both aminopyridine rings, one to Glu592 and the other to heme propionate D (Figure S4A of the Supporting Information). However, in eNOS, one aminopyridine hydrogen bonds with Glu363, but the second aminopyridine does not hydrogen bond with heme propionate D because Tyr477 does not rotate out of the way (Figure S4B of the Supporting Information).

#### Is the Tyr Position the Sole Determinant for Inhibitor Binding?

The common structural feature with these inhibitors is that the conserved Tyr adopts the out-rotamer conformation in nNOS, thus allowing one aminopyridine to form the bifurcated hydrogen bonds with heme propionate D, while in eNOS, the Tyr remains in the in-rotamer position. To determine if the Tyr side chain position is the sole determinant of the isoform-dependent inhibitor binding mode, we have prepared the eNOS Y477A mutant and determined crystal structures of the mutant bound with two inhibitors that do not disturb the Tyr477 rotamer in wild type eNOS. As shown in Figure 4A, the binding mode of (3*R*,4*R*)-3 is the same as that in wild type eNOS (Figure 3B); that is, the aminopyridine makes only one hydrogen bond with heme propionate D. The only difference is that the void left by the smaller side chain of Ala477 allows the aminopyridine ring to fill in the space, thereby losing its hydrogen bond to Asn430 (Figure 4A).

In contrast, the structure of eNOS Y477A bound with (2*R*,4*S*)-6 provides a clear-cut case in which the Tyr477 side chain alone fully controls how (2*R*,4*S*)-6 binds, while in wild type eNOS, (2*R*,4*S*)-6 cannot hydrogen bond with heme propionate D because the Tyr477 side chain blocks the position of heme propionate D. When the Tyr side chain is absent in the Y477A mutant, (2*R*,4*S*)-6 is able to take the place of Tyr477 (Figure 4B). This resembles the binding mode observed in the nNOS-6 structure (Figure S3A of the Supporting Information) but lacking the stacking interaction between the aminopyridine ring and the Tyr side chain. Interestingly, the determinations of  $K_s$  (Table 2) indicate that being able to make bifurcated H-bonds from the aminopyridine to heme propionate D alone does not increase the affinity of (2*R*,4*S*)-6 for eNOS Y477A compared to that of wild type eNOS. This implies that stacking of the aminopyridine ring with the Tyr side chain in its out-rotamer position also contributes to the binding of (2*R*,4*S*)-6, which is the case in the nNOS-6 structure (Figure S3A of the Supporting Information). Removing the Tyr side chain does not lead to tighter binding even though it allows the inhibitor's aminopyridine to H-bond with heme propionate D. Rather, allowing

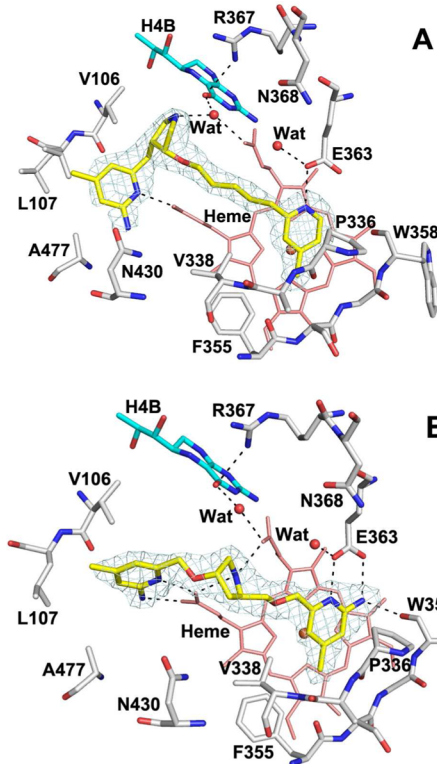


**Figure 4.** eNOS Y447A mutant active site bound with (A) (3*R*,4*R*)-3 and (B) (2*R*,4*S*)-6. The omit  $F_o - F_c$  density map for each inhibitor is shown at the 3.0 $\sigma$  contour level. Major hydrogen bonds are depicted as dashed lines.

the Tyr to adopt an out-rotamer position is the key to better binding affinity for inhibitors discussed in this study.

**Reasons for the Different Tyr Mobilities.** What remains to be explained is why the highly conserved Tyr residue, among different species and across the NOS isoforms, is more mobile in rat nNOS than in bovine eNOS. The protein environment near the Tyr is different in the two isoforms, with Met336 in nNOS versus Val106 in eNOS being one of the more obvious differences. When the aminopyridine hydrogen bonds with heme propionate D, Met336 is able to form more extensive contacts with the inhibitor in nNOS than would be possible for Val106 in eNOS. This could help to provide the energetic incentive for the conserved Tyr to move away in nNOS. In addition, the larger Met336 in nNOS may make it less favorable because of steric crowding of the inhibitor, such as (3*R*,4*R*)-2 and (3*R*,4*R*)-3, preventing adoption of the extended conformation, as observed in eNOS. To test this interpretation, we determined the structures of (3*R*,4*R*)-2 and (3*R*,4*R*)-3 bound to the nNOS M336V/D597N mutant that mimics eNOS. There is very little difference in the way (3*R*,4*R*)-2 binds to the mutant and wild type with the exception of the pyrrolidine moiety (Figure 5A). More complex is how (3*R*,4*R*)-3 binds to the nNOS mutant (Figure 5B). Two alternate conformations are required to properly model the electron density for the aminopyridine and pyrrolidine rings. One conformation is the one already observed in the wild type nNOS-3 structure with the pyrrolidine ring extending out and the aminopyridine forming bifurcated hydrogen bonds with heme propionate D. The other conformation is the same as that seen in the eNOS-3 structure with the aminopyridine hydrogen bonded with both heme and Asn340. The Tyr706 side chain must have two alternate rotamer

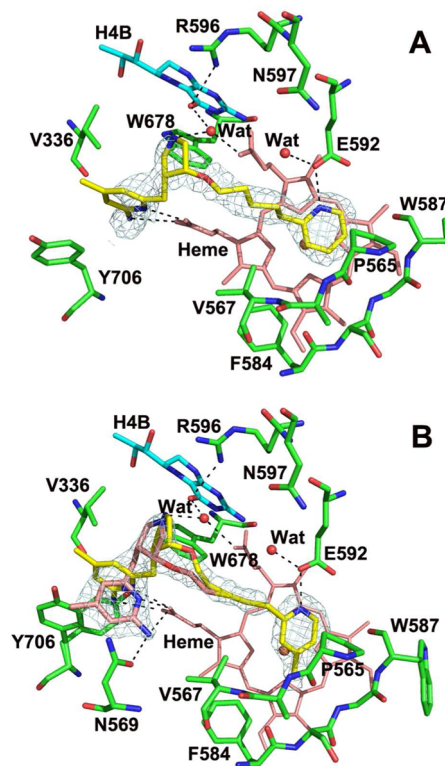


**Figure 5.** Active site of the nNOS M336V/D597N mutant bound with (A) (3R,4R)-2 and (B) (3R,4R)-3. The aminopyridine and pyrrolidine moieties in (3R,4R)-3 adopt two conformations (yellow and pink) in nNOS. The Tyr706 side chain also has two conformations to accommodate the inhibitor. The omit  $F_o - F_c$  density map is contoured at  $3.0\sigma$  for each inhibitor. Major hydrogen bonds are depicted as dashed lines.

conformations to accommodate the inhibitor's aminopyridine moiety in two different positions (Figure 5B). Although the Met to Val substitution indeed has some impact on how the inhibitor interacts with the enzyme, we observed slightly weaker binding of (3R,4R)-2 and (3R,4R)-3 to the nNOS M336V/D597N mutant (Table 2), but inhibitor binding conformations in the nNOS M336V/D597N mutant do not fully mimic inhibitor conformations in the eNOS-2 or -3 structure.

What complicates the mobility of the conserved Tyr is that an extended segment of disordered polypeptide in both eNOS and nNOS (residues 339–349 in nNOS or residues 109–120 in eNOS) differs in both sequence and length and thus could also contribute to dynamical differences in eNOS and nNOS. In the eNOS-3 structure and a few others, we were able to observe density for a few more residues, and thus, we could model Arg109–Leu111 in the usually disordered region, as shown in Figure 6. In addition, with some inhibitors, this region is visible in electron density maps of nNOS. One example is the nNOS structure (PDB entry 4JSH) where the normally disordered segment was fully modeled with the  $2F_o - F_c$  density contoured at  $0.5\sigma$  (Figure 7). The backbone of the loop in nNOS resembles the fully ordered region observed in the human iNOS structure (PDB entry 1NSI); that is, residues from Pro338 to Thr342 form a  $3_{10}$  helix. This additional information shows that the backbone of this N-terminal portion in eNOS heme domain is packed more tightly against the C-terminal fragment where Tyr477 is located. Additional mutants in this region suggest that it is indeed how the backbone packs near the conserved Tyr but not specific amino

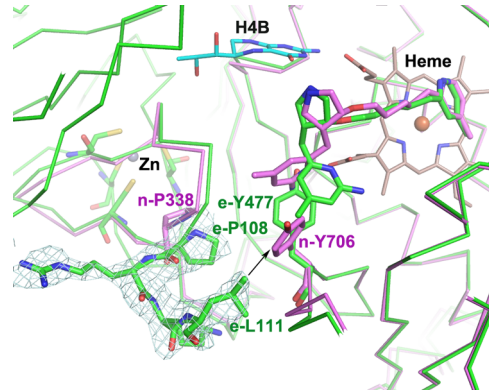


**Figure 6.** Superimposition of the nNOS-3 structure (purple, shown as one subunit only) on the eNOS-3 structure (green) locally around the heme active site (Pro565–Asp600 in nNOS vs Pro336–Asp371 in eNOS). In nNOS, the loop after Pro338 is invisible, while in eNOS, the loop is ordered up to Leu111, as indicated by the  $2F_o - F_c$  density contoured at  $0.8\sigma$ . Different binding conformations of (3R,4R)-3 are shown with the Tyr residue swung out (nNOS, purple) or not (eNOS, green). The potential steric clash between Leu111 and Tyr477 in its assumed out-rotamer position is indicated by an arrow.

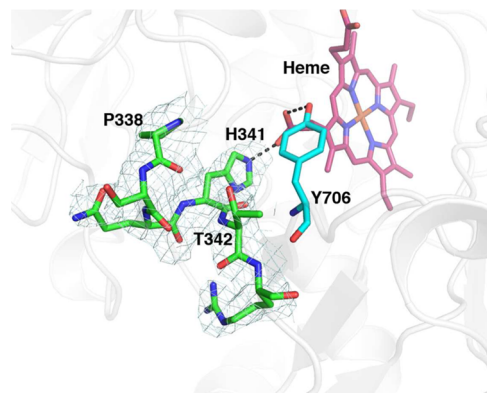


**Figure 7.** Segment adjacent to the Tyr706-residing fragment. The normally disordered polypeptide (residues 339–349) becomes partially ordered in certain nNOS structures (PDB entry 4JSH). The  $2F_o - F_c$  electron density is contoured at  $0.5\sigma$  around the  $3_{10}$  helix in the segment.

acid differences that control the Tyr rotamer conformation. For example, Leu111 in eNOS is in position to possibly clash with the out-rotamer conformation of Tyr477, but the eNOS L111A mutant in complexes with (3R,4R)-3 or (3R,4R)-5 shows that Tyr477 remains in place and does not adopt the out-rotamer conformation (Figure S5 of the Supporting Information). The  $K_s$  of (3R,4R)-3 with eNOS L111A shows a binding affinity 7-fold tighter than that of wild type eNOS (Table 2). Even though this mutation does not impact the Tyr477 side chain rotamer position, it may affect inhibitor binding by providing a distorted packing between the N-terminal portion and the Tyr477-residing C-terminal fragment that lines up the active site entrance. Another interaction unique in nNOS is His341 (Leu in eNOS), which H-bonds with heme propionate D; this could possibly weaken the Tyr706–heme propionate interaction, thus allowing Tyr706 to more easily adopt the out-rotamer conformation. However, Tyr706 in the H341L mutant complexed with (3R,4R)-2 or (2R,4S)-6 still adopts the out-rotamer conformation (Figure S6 of the Supporting Information) just as it does in wild type nNOS. We did see weaker binding of (2R,4S)-6 to the H341L mutant of nNOS compared to that of the wild type in the

$K_s$  measurement, but the binding is still tighter than that to eNOS (Table 2), which is consistent with the double-headed binding observed in the nNOS H341L–6 structure.

One final example supporting the conformational mobility of the polypeptide and not specific amino acid differences as the key factor controlling the mobility of the conserved Tyr stems from the structure of human iNOS complexed with 7. As noted, the backbone conformation of the polypeptide in this region is the same in both nNOS and iNOS, but in iNOS, this region is fully ordered with well-defined electron density. When 7 binds to nNOS, Tyr706 adopts the out-rotamer conformation, but in iNOS, the corresponding Tyr491 remains in place (Figure 8).

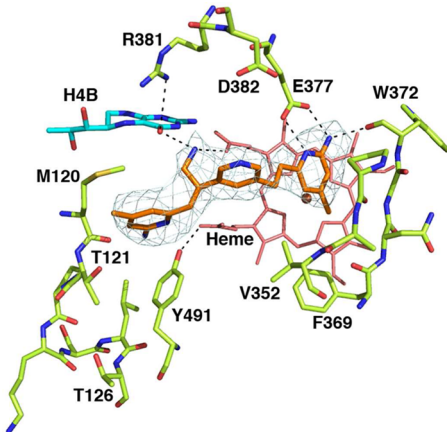


**Figure 8.** Active site of human iNOS with 7 bound. The omit  $F_o - F_c$  density map is contoured at  $3.0\sigma$  for the inhibitor. Major hydrogen bonds are depicted as dashed lines. The second aminopyridine of 7 is far from heme propionate D, which itself makes an H-bond with Tyr491 in an in-rotamer position.

Indeed, if Tyr491 were to adopt the out-rotamer conformation, there would be potential steric clashes with Thr126 unless the Thr126 segment would move, which, apparently, does not happen in iNOS. Interestingly, Tyr491 of iNOS is more resistant to the out-rotamer position than is Tyr477 in eNOS because, when 7 binds, both Tyr477 in eNOS and Tyr706 in nNOS adopt an out-rotamer position to allow one of the two aminopyridines of 7 to form bifurcated H-bonds with heme propionate D, as shown in Figure S7 of the Supporting Information. Note, too, that 7 is a more potent inhibitor of iNOS than of eNOS but not of nNOS. We previously have shown that there is greater electrostatic stabilization of 7 bound to nNOS than eNOS because of a single amino acid difference: Asp597 in nNOS is Asn368 in eNOS (see Figures 2 and 3).<sup>12</sup> This residue is Asp382 in iNOS, which explains why 7 is ~6-fold better at inhibiting iNOS than eNOS. However, 7 is an ~95-fold better inhibitor of nNOS than of iNOS. Because the electrostatic properties of iNOS and nNOS are so similar, the better potency of 7 for nNOS supports the view that the ability of the Tyr to adopt the out-rotamer conformation in nNOS plays a major role in inhibitor potency. The two main reasons why the out-rotamer conformation results in better potency are that H-bonds between the inhibitor aminopyridine and heme propionate are optimized and aromatic stacking occurs between the Tyr out-rotamer conformation and inhibitor aminopyridine.

## CONCLUSIONS

The Tyr706 side chain in nNOS can easily adopt an out-rotamer position when pyrrolidine-based inhibitors bind to the active site, while Tyr477 tends to remain in place in eNOS structures. The structural basis for this isoform-dependent difference in Tyr mobility cannot be attributed to any single residue in the often disordered region near the conserved Tyr. The backbone structure of this region is basically the same in nNOS and iNOS based on the available information. Even so, in iNOS this region exhibits well-defined electron density and clearly is more highly ordered than in nNOS. The out-rotamer position of the conserved Tyr requires flexibility in this region, which happens to be rigid in iNOS. This segment, however, adopts a different backbone structure in eNOS compared to iNOS and nNOS, and despite the relatively high mobility of this region, the polypeptide is closer to the conserved Tyr in eNOS, thus presenting a greater energy barrier to the conserved Tyr adopting the out-rotamer conformation. In addition, the Met336 (nNOS) to Val106 (eNOS) substitution can influence the binding of inhibitors such as (3*R*,4*R*)-2 and (3*R*,4*R*)-3. These different binding modes in nNOS and eNOS, caused by the Tyr residue mobility, have proven to be the basis for the sharp differences in inhibitor potency (Table 1). Therefore, the mobility of this Tyr residue can be utilized in the future development of isoform selective NOS inhibitors.

## ASSOCIATED CONTENT

### Supporting Information

Table of crystallographic data collection and structure refinement statistics (with PDB entries),  $K_s$  titration curve fittings, and other structural figures. This material is available free of charge via the Internet at <http://pubs.acs.org>.

### Accession Codes

eNOS–2, 4CWV; eNOS–3, 4CWW; eNOS–4, 4CWX; eNOS–5, 4CWY; eNOS Y477A–3, 4CWZ; eNOS Y477A–6, 4CX0; eNOS L111A–3, 4CX1; eNOS L111A–5, 4CX2; nNOS M336V/D597N–2, 4CX3; nNOS M336V/D597N–3, 4CX4; nNOS H341L–2, 4CX5; nNOS H341L–6, 4CX6; iNOS–7, 4CX7.

## AUTHOR INFORMATION

### Corresponding Authors

\*E-mail: poulos@uci.edu. Phone: (949) 824-7020.

\*E-mail: agman@chem.northwestern.edu. Phone: (847) 491-5653. Fax: (847) 491-7713.

### Present Addresses

<sup>§</sup>S.D.: Celgene, 4550 Towne Centre Ct., San Diego, CA 92121.

<sup>||</sup>H.J.: Department of Chemistry, University of Utah, Salt Lake City, UT 84112.

### Funding

This work was supported by National Institutes of Health Grants GM057353 to T.L.P. and GM049725 to R.B.S.

### Notes

The authors declare no competing financial interest.

## ACKNOWLEDGMENTS

H.L. thanks Victoria S. Jasion and Yarrow Modrona for their help in X-ray data collection. We also thank the beamline staff at SSRL and ALS for their assistance during the remote X-ray diffraction data collection.

## ABBREVIATIONS

NO, nitric oxide; nNOS, neuronal nitric oxide synthase; iNOS, inducible nitric oxide synthase; eNOS, endothelial nitric oxide synthase; H<sub>4</sub>B, tetrahydrobiopterin; GSH, reduced glutathione; MES, 2-(N-morpholino)ethanesulfonic acid; HEPES, 2-[4-(2-hydroxyethyl)piperazin-1-yl]ethanesulfonic acid; TCEP, tris(2-carboxyethyl)phosphine; PDB, Protein Data Bank.

## REFERENCES

- (1) Stuehr, D. J., and Griffith, O. W. (1992) Mammalian nitric oxide synthases. *Adv. Enzymol. Relat. Areas Mol. Biol.* 65, 287–346.
- (2) Moncada, S., Palmer, R. M., and Higgs, E. A. (1991) Nitric oxide: Physiology, pathophysiology, and pharmacology. *Pharmacol. Rev.* 43, 109–142.
- (3) Hobbs, A. J., Higgs, A., and Moncada, S. (1999) Inhibition of nitric oxide synthase as a potential therapeutic target. *Annu. Rev. Pharmacol. Toxicol.* 39, 191–220.
- (4) Silverman, R. B. (2009) Design of selective neuronal nitric oxide synthase inhibitors for the prevention and treatment of neurodegenerative diseases. *Acc. Chem. Res.* 42, 439–451.
- (5) Poulos, T. L., and Li, H. (2013) Structural basis for isoform-selective inhibition in nitric oxide synthase. *Acc. Chem. Res.* 46, 390–398.
- (6) Calabrese, V., Bates, T. E., and Stella, A. M. (2000) NO synthase and NO-dependent signal pathways in brain aging and neurodegenerative disorders: The role of oxidant/antioxidant balance. *Neurochem. Res.* 25, 1315–1341.
- (7) Taddei, S., Virdis, A., Ghiaconi, L., Sudano, I., and Salvetti, A. (2001) Endothelial dysfunction in hypertension. *J. Cardiovasc. Pharmacol.* 38 (Suppl. 2), S11–S14.
- (8) Crane, B. R., Arvai, A. S., Ghosh, D. K., Wu, C., Getzoff, E. D., Stuehr, D. J., and Tainer, J. A. (1998) Structure of nitric oxide synthase oxygenase dimer with pterin and substrate. *Science* 279, 2121–2126.
- (9) Raman, C. S., Li, H., Martasek, P., Kral, V., Masters, B. S., and Poulos, T. L. (1998) Crystal structure of constitutive endothelial nitric oxide synthase: A paradigm for pterin function involving a novel metal center. *Cell* 95, 939–950.
- (10) Fischmann, T. O., Hruza, A., Niu, X. D., Fossetta, J. D., Lunn, C. A., Dolphin, E., Prongay, A. J., Reichert, P., Lundell, D. J., Narula, S. K., and Weber, P. C. (1999) Structural characterization of nitric oxide synthase isoforms reveals striking active-site conservation. *Nat. Struct. Biol.* 6, 233–242.
- (11) Li, H., Shimizu, H., Flinspach, M., Jamal, J., Yang, W., Xian, M., Cai, T., Wen, E. Z., Jia, Q., Wang, P. G., and Poulos, T. L. (2002) The novel binding mode of N-alkyl-N'-hydroxyguanidine to neuronal nitric oxide synthase provides mechanistic insights into NO biosynthesis. *Biochemistry* 41, 13868–13875.
- (12) Flinspach, M. L., Li, H., Jamal, J., Yang, W., Huang, H., Hah, J. M., Gomez-Vidal, J. A., Litzinger, E. A., Silverman, R. B., and Poulos, T. L. (2004) Structural basis for dipeptide amide isoform-selective inhibition of neuronal nitric oxide synthase. *Nat. Struct. Mol. Biol.* 11, 54–59.
- (13) Huang, H., Martasek, P., Roman, L. J., and Silverman, R. B. (2001) Synthesis and evaluation of dipeptide amides containing N<sup>ω</sup>-nitroarginine and D-2,4-diaminobutyric acids as inhibitors of neuronal nitric oxide synthase. *J. Enzyme Inhib.* 16, 233–239.
- (14) Huang, H., Martasek, P., Roman, L. J., Masters, B. S., and Silverman, R. B. (1999) N<sup>ω</sup>-Nitroarginine-containing dipeptide amides. Potent and highly selective inhibitors of neuronal nitric oxide synthase. *J. Med. Chem.* 42, 3147–3153.
- (15) Ji, H., Stanton, B. Z., Igarashi, J., Li, H., Martasek, P., Roman, L. J., Poulos, T. L., and Silverman, R. B. (2008) Minimal pharmacophoric elements and fragment hopping, an approach directed at molecular diversity and isozyme selectivity. Design of selective neuronal nitric oxide synthase inhibitors. *J. Am. Chem. Soc.* 130, 3900–3914.
- (16) Delker, S. L., Ji, H., Li, H., Jamal, J., Fang, J., Xue, F., Silverman, R. B., and Poulos, T. L. (2010) Unexpected binding modes of nitric oxide synthase inhibitors effective in the prevention of a cerebral palsy phenotype in an animal model. *J. Am. Chem. Soc.* 132, 5437–5442.
- (17) Ji, H., Delker, S. L., Li, H., Martasek, P., Roman, L. J., Poulos, T. L., and Silverman, R. B. (2010) Exploration of the active site of neuronal nitric oxide synthase by the design and synthesis of pyrrolidinomethyl 2-aminopyridine derivatives. *J. Med. Chem.* 53, 7804–7824.
- (18) Delker, S. L., Xue, F., Li, H., Jamal, J., Silverman, R. B., and Poulos, T. L. (2010) Role of zinc in isoform-selective inhibitor binding to neuronal nitric oxide synthase. *Biochemistry* 49, 10803–10810.
- (19) Xue, F., Fang, J., Delker, S. L., Li, H., Martasek, P., Roman, L. J., Poulos, T. L., and Silverman, R. B. (2011) Symmetric double-headed aminopyridines, a novel strategy for potent and membrane-permeable inhibitors of neuronal nitric oxide synthase. *J. Med. Chem.* 54, 2039–2048.
- (20) Huang, H., Ji, H., Li, H., Jing, Q., Labby, K. J., Martasek, P., Roman, L. J., Poulos, T. L., and Silverman, R. B. (2012) Selective monocationic inhibitors of neuronal nitric oxide synthase. Binding mode insights from molecular dynamics simulations. *J. Am. Chem. Soc.* 134, 11559–11572.
- (21) Isin, E. M., and Guengerich, F. P. (2006) Kinetics and thermodynamics of ligand binding by cytochrome P450 3A4. *J. Biol. Chem.* 281, 9127–9136.
- (22) McMillan, K., and Masters, B. S. (1993) Optical difference spectrophotometry as a probe of rat brain nitric oxide synthase heme-substrate interaction. *Biochemistry* 32, 9875–9880.
- (23) Berka, V., Chen, P. F., and Tsai, A. L. (1996) Spatial relationship between L-arginine and heme binding sites of endothelial nitric-oxide synthase. *J. Biol. Chem.* 271, 33293–33300.
- (24) Blasko, E., Glaser, C. B., Devlin, J. J., Xia, W., Feldman, R. I., Polokoff, M. A., Phillips, G. B., Whitlow, M., Auld, D. S., McMillan, K., Ghosh, S., Stuehr, D. J., and Parkinson, J. F. (2002) Mechanistic studies with potent and selective inducible nitric-oxide synthase dimerization inhibitors. *J. Biol. Chem.* 277, 295–302.
- (25) McPhillips, T. M., McPhillips, S. E., Chiu, H. J., Cohen, A. E., Deacon, A. M., Ellis, P. J., Garman, E., Gonzalez, A., Sauter, N. K., Phizackerley, R. P., Soltis, S. M., and Kuhn, P. (2002) Blu-Ice and the Distributed Control System: Software for data acquisition and instrument control at macromolecular crystallography beamlines. *J. Synchrotron Radiat.* 9, 401–406.
- (26) Otwinowski, Z., and Minor, W. (1997) Processing of X-ray diffraction data collected in oscillation mode. *Methods Enzymol.* 276, 307–326.
- (27) Kabsch, W. (2010) Xds. *Acta Crystallogr. D66*, 125–132.
- (28) Evans, P. R. (2006) Scaling and assessment of data quality. *Acta Crystallogr. D62*, 72–82.
- (29) Murshudov, G. N., Vagin, A. A., and Dodson, E. J. (1997) Refinement of Macromolecular Structures by the Maximum-Likelihood Method. *Acta Crystallogr. D53*, 240–255.
- (30) Emsley, P., and Cowtan, K. (2004) Coot: Model-building tools for molecular graphics. *Acta Crystallogr. D60*, 2126–2132.
- (31) Winn, M. D., Isupov, M. N., and Murshudov, G. N. (2001) Use of TLS parameters to model anisotropic displacements in macromolecular refinement. *Acta Crystallogr. D57*, 122–133.
- (32) Jing, Q., Li, H., Roman, L. J., Martasek, P., Poulos, T. L., and Silverman, R. B. (2014) An Accessible Chiral Linker to Enhance Potency and Selectivity of Neuronal Nitric Oxide Synthase Inhibitors. *ACS Med. Chem. Lett.* 5, 56–60.
- (33) Holden, J. K., Li, H., Jing, Q., Kang, S., Richo, J., Silverman, R. B., and Poulos, T. L. (2013) Structural and biological studies on bacterial nitric oxide synthase inhibitors. *Proc. Natl. Acad. Sci. U.S.A.* 110, 18127–18131.
- (34) Kang, S., Tang, W., Li, H., Chreifi, G., Martasek, P., Roman, L. J., Poulos, T. L., and Silverman, R. B. (2014) Nitric oxide synthase inhibitors that interact with both heme propionate and tetrahydrobiopterin show high isoform selectivity. *J. Med. Chem.* 57, 4282–4296.